Measurement 46 (2013) 1125–1136

Contents lists available at SciVerse ScienceDirect

Measurement

journal homepage: www.elsevier.com/locate/measurement

Passive control of circular cylinder wake in shallow flow

Bengi Gozmen, Huseyin Akilli *, Beşir Sahin

Cukurova University, Department of Mechanical Engineering, 01330 Yüreğir, Adana, Turkey

ARTICLE INFO

Article history:
Received 2 May 2012
Received in revised form 30 October 2012
Accepted 4 November 2012
Available online 2 December 2012

Keywords:
PIV
Shallow water
Splitter plate
Vortex shedding

ABSTRACT

The control of vortex shedding of a circular cylinder in shallow water using a splitter plate located in the downstream of the circular cylinder was studied by employing particle image velocimetry (PIV) technique. Experiments were carried out in a water channel having a test section of 8000 mm × 1000 mm × 750 mm dimensions at a Reynolds number of 6250. The length of the splitter plate (L) was varied within the range of $0.5 \leqslant L/D \leqslant 2$ with an increment of 0.5. The plate was submerged into water at different height ratios (h_p/h_w) such as 0.25, 0.5, 0.75 and 1.0. Mean velocity vector field, corresponding vorticity contours, streamline topologies and turbulent quantities were calculated using 300 instantaneous velocity vector field measured by PIV. As the ratio of h_p/h_w increases, the effect of the splitter plate on the suppression of the vortex shedding increases. Flow characteristics and examination of spectra indicate that Karman vortex shedding is attenuated pronouncedly for the cases of $L/D \geqslant 1$ and $h_p/h_w \geqslant 0.75$. The transverse Reynolds normal stress is more effective on the attenuation of turbulent kinetic energy than the streamwise Reynolds normal stress. The value of peak transverse Reynolds normal stress is reduced to 90% of that of the bare cylinder at most.

1. Introduction

The phenomenon of vortex shedding from a cylinder is a challenging and an interesting problem in fluid dynamics and engineering applications. The wake behind the cylinder can generate large unsteady forces which have the potential to damage structures downstream of the cylinder. Because of its practical importance, methods of attenuation of vortex shedding from bluff bodies have been widely studied numerically and experimentally. Many excellent studies on the flow structure downstream of bluff bodies can be found in the reviews of Choi et al. [24] and Williamson [25].

There are two main methods to control the unsteady flow structure on the bluff bodies: active and passive control. Active control methods, apply some sorts of energy into the flow field. Many active control techniques have been applied to unsteady flow, such as feedback control [1], electro-magnetic control [2], rotary oscillation of cylinder [3–5] and suction and blowing [6–8]. Passive control techniques have been developed to control the vortex shedding by modifying the shape of the bluff body or by attaching additional devices in the flow field without any input of external energy. The most used techniques of passive control are splitter plate [9–14], control cylinders [15], surface protrusion [16,17] and base bleed [18].

A shallow water flow is defined as the condition that the horizontal length scale of the flow is significantly larger than its vertical length scale (usually the depth). Many wake flows in nature such as in wide rivers, lakes, estuaries, shallow coastal waters, or mountains can be given as examples of shallow turbulent flows. Ingram and Chu [19] studied on the effect of bottom friction around an island. When transverse shear was large, a vortex street wake was formed like in flows around small islands. On the other hand, for small transverse shear, the shear layer was stabilized by bottom friction as in the flows around large islands. The study of Chen and Jirka [20] denoted that flow structure downstream of bluff bodies in shallow

* Corresponding author. Tel.: +90 5332372129; fax: +90 3223386126.
E-mail address: hakilli@cu.edu.tr (H. Akilli).

0263-2241/$ - see front matter © 2012 Elsevier Ltd. All rights reserved.
http://dx.doi.org/10.1016/j.measurement.2012.11.008

Nomenclature

D	cylinder diameter	y	transverse coordinate
L	splitter plate length	ω	spanwise vorticity
h_w	water height	$u'v'$	Reynolds shear stress correlation
h_p	the plate height in the water	$v'v'$	transverse Reynolds normal stress
L_s	location of saddle point	$u'u'$	streamwise Reynolds normal stress
Re	Reynolds number	S	spectra of streamwise velocity fluctuation
U	free-stream velocity	Sa	saddle point
x	streamwise coordinate		

water is different from that in deep water. Akilli et al. [21] investigated the effects of the side-by-side cylinders on the flow structure in shallow water. They obtained that jet-like flow between the cylinders was considerable effective for small gap ratios ($G/D \leqslant 1.5$) particularly for the gap ratio of $G/D = 1.25$. Akilli and Rockwell [22] studied the flow characteristics downstream of a vertical circular cylinder in shallow water flow using the Particle Image Velocimetry (PIV) technique. They showed that near the bed, the time-averaged streamline topology downstream of the base of the cylinder resembled an owl face, which was originally defined for a completely different exterior flow. At locations above the bed, one of the two principle saddle points of the owl face of the first kind disappeared and the principle foci were transformed from a stable to an unstable state. The study of Fu and Rockwell [18] showed that shallow flow past a cylinder gave rise to a horseshoe vortex system about the upstream surface of the cylinder, and large-scale vortex formation in the near wake.

The reviews mentioned so far were based on the principal of that the shallowness ensures 2D (two dimensional) turbulence. Besides these, some researchers observed that shallow flows exhibit complex three-dimensional (3D) structures. The study of Akkermans et al. [26] revealed that significant and remarkably complex 3D structures and vertical motions appeared throughout the flow evolution, i.e., during and after the forcing face. The bottom friction and free surface deformation were not the main mechanisms to generate three-dimensional (3D) structure. The investigation of Akkermans et al. [27] represented that the vertical recirculation associated with the three-dimensional structure was due to the vertical confinement of the flow. Akkermans et al. [28] studied on the 3D structure of a linear array of vortices in a shallow layer. They observed that 3D flow structure led to dispersion of passive tracers that differs from that in 2D flows. Sous et al. [29] focused on transition from deep to shallow water layer. They defined a number C characterizing the vertical confinement. Their experiments indicated that the generated turbulence was a typical three-dimensional turbulence when $C < 1$. For $C > 2$, a particular behavior appeared where the flow was quasi-two dimensional (Q2D). Lin et al. [30] studied on space–time development of instantaneous flow characteristics along planes indicating 3D vortex structure. Their study showed that the quasi-two dimensional patterns evolved to different forms depending on the depth of shallow water.

The splitter plate is one of the most successful passive control techniques that is used to control vortex shedding downstream of the cylinder. Cimbala and Garg [10] investigated the effect of the attached splitter plate on the flow characteristics downstream of a fixed cylinder and a freely rotating cylinder. The effect of fixed cylinder with an attached plate was similar to the case of a freely rotating cylinder, the flow field with plate of $L/D > 2$. However, when $L/D < 2$, the flow field was similar to the case without the splitter plate. They also showed for the case of a fixed cylinder that the Strouhal number increased for $1 < L/D < 2$, but the Strouhal number decreased as the length of the plate further increased. The study of Cardell [11] showed that the introduction of low solidity splitter plates did not change the basic near wake structure and that sufficiently high solidity uncoupled the large scale wake instability from the body with the primary vortex formation occurring downstream of the separation bubble due to instability of the wake profile. The permeable splitter plates reduced the drag and modified the primary wake frequency. Kwon and Choi [12] studied the control of laminar vortex shedding downstream of a circular cylinder using splitter plates. They revealed that the vortex shedding downstream of a circular cylinder completely disappeared when the length of the splitter plate was longer than a critical length, and this critical length was proportional to the Reynolds number. The Strouhal number rapidly decreased with the increased plate length until $L/D \approx 1$ and showed two different behaviors at $1 < L/D < 2$. Ozono's study [9] indicated that the vortex shedding could be suppressed even when the splitter plates were arranged asymmetrically downstream of the cylinder and the length of splitter plate did not have much effect on the flow structure in the case of asymmetric arrangement. Akilli et al. [13] investigated the thickness effect of splitter plate on the suppression of vortex shedding in shallow water by using the PIV Technique. Their study denoted that the change in the splitter plate thicknesses did not have any considerable effect on the flow structure. The splitter plate had a substantial effect on suppression of the vortex shedding for the gap ratio (the distance between the base of cylinder and the leading edge of the splitter plate) between 0 and $1.75D$. When the splitter plate was located at 2D location, no effect of the splitter plate was observed. Akilli et al. [14] researched the flow characteristics of the wakes downstream of the circular cylinder by attaching splitter plates. Their work indicated that the frequency of vortex

shedding decreased until the length of $L/D = 0.6$ by lengthening the used splitter plate. Because of the stabilizing effect of the shallow water, the dominant frequency of the shedding vortices was not obtained after the case of $L/D = 0.6$. After the length of $L/D = 1.2$, the changes in the turbulent kinetic energy, Reynolds shear and normal stress patterns were inconsiderable. Over this critical length $L/D = 1.2$, the large scale vortex shedding downstream of the cylinder was vanished.

The main objective of this experimental study is to reveal the interaction of vortices emanating from a circular cylinder with a splitter plate having different lengths and heights in the shallow water. In particular, we would like to answer the following question: how does a submerged attachment change the flow structure behind bluff bodies in shallow water flows? Can dispersion of contamination in transverse direction in shallow flows, due to Karman vortices, be prevented by suppressing the flow oscillations downstream of a bluff body? In line with this objective, splitter plates having various lengths and heights were placed downstream of the circular cylinder. The present work reveals details of flow structure downstream of a circular cylinder in shallow flow experimentally using the particle image velocimetry technique.

2. Experimental setup

Experiments were carried out in a closed loop shallow water channel. The test section which is made of transparent plexiglass material has a length of 8000 mm, a width of 1000 mm and a height of 750 mm. A schematic view of experimental setup in the plan view and side view planes is shown in Fig. 1. A centrifugal pump with a speed control unit drives the flow. The cylinder used during the experiments was made of plexiglass material and its diameter D was 50 mm, and the length of splitter plates were $D/2$, D, $3D/2$, $2D$. Splitter plates, having a width of 4 mm, were also made of plexiglass material. In order to understand the effect of submerged height of the splitter plate, four height ratios, h_p/h_w such as 0.25, 0.5, 0.75 and 1.0 were used. The water level h_w was maintained at the height of 25 mm and the flow characteristics were measured at mid-depth of the water. Experiments were carried out at a free-stream velocity of 0.125 m/s corresponding to the Reynolds number based on the cylinder diameter of Re = 6250. At these flow conditions, the value of Froude number (Fr) is 0.064 which is an indication of no surface distortion in the flow field. Trip wires were located at the leading edge of the platform to provide fully-developed turbulent velocity profile at the location of interest. The cylinder and plates were located at 1750 mm from the leading edge of the platform. The splitter plate was attached on the base of the circular cylinder. In order to obtain instantaneous velocity vectors and related flow characteristics, the PIV technique was employed. The flow field illumination was provided by two Nd:YAG pulsed laser sources with a wave length of 532 nm, each with a maximum energy output of 120 mJ/pulse. Dantec flow map processor, that controlled the timing of the data acquisition, was used to synchronize the image acquisition and laser unit. The thickness of the laser sheet illuminating the flow field was approximately 1.5 mm. The water was seeded with the neutrally buoyant spherical particles of 12 μm in diameter and the particle density was about 1100 kg/m^3. The Stokes Number of the particles which provides a measure of the ability of particles to track the flow field is calculated about 1.83×10^{-4} [33]. Therefore, this value indicates that the particles in these experiments follow the streamlines precisely. The movement of the particles was recorded by a CCD camera with a resolution 1024×1024 pixels. The camera was equipped with a 55 mm focal-length lens. Dantec flow grabber digital PIV software employing frame-to-frame adaptive correlation technique was used to calculate the raw displacement vector field from the particle image velocity data. Cross-correlation technique was employed to calculate the raw displacement vector field from the particle image velocity data. In the image processing, 32×32 pixels rectangular effective interrogation windows were used. During the interrogation process, an overlap of 50% was employed in order to satisfy Nyguist criterion. In the post-processing step, interpolation between surrounding vectors was used in order to remove erroneous vectors and replacement. Displacement of vector field and velocity vectors of the flow could be measured and calculated, respectively. The vorticity patterns of the wake flow could be calculated from the circulation using a finite difference scheme. The overall field of view was 160×160 mm^2 ($3.2D \times 3.2D$). This type of view provided better observation of the data for which a large domain was covered. For all experiments 300 instantaneous images were taken. Patterns of instantaneous particle images were taken at a rate of 15 Hz, thereby spanning 13.4 s. Averaged patterns of the flow structure were calculated from this total number of instantaneous images. A software developed in-house were used to complete the velocity vector field, streamline topology and other turbulent statistics. The uncertainties for velocity

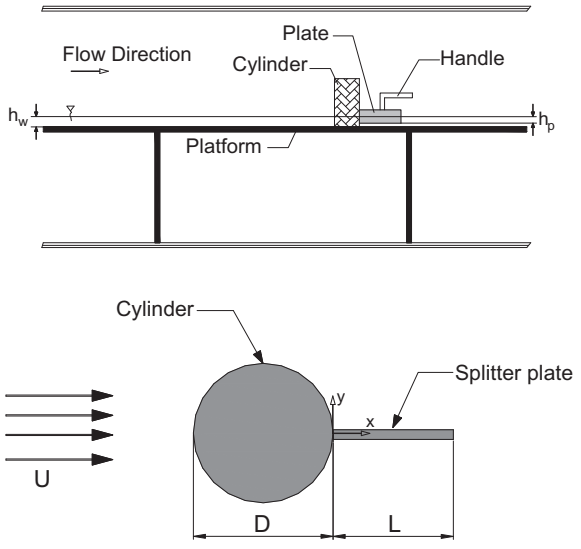

Fig. 1. Shematic of the experimental system and definition of the parameters: cylinder diameter D, length of plate L, plate height in water h_p, water height h_w and free-stream velocity U.

and related turbulent statistics were estimated as 3% and 5%, respectively.

3. Results and discussion

3.1. Flow patterns: velocity vector field, spanwise vorticity and Reynolds shear stress contours

The flow structure of the near wake behind a bare circular cylinder is displayed in Fig. 2 to compare the flow characteristics with the presence of the splitter plate cases. To explain the flow structure, the time-averaged velocity vector field $\langle U \rangle$, patterns of spanwise vorticity contours $\langle \omega \rangle$ and Reynolds shear stress $\langle u'v' \rangle / U^2$ are demonstrated in Fig. 2. The saddle point *Sa*, which explicitly indicates the location of stagnation point and the size of the wake region is located with a distance of approximately one cylinder diameter far from the base of the cylinder. In terms of spanwise vorticity patterns downstream of the bare cylinder, the vorticity remains condensed near the cylinder. Both negative vorticity shown by dashed lines and positive vorticity shown by solid lines extend in streamwise direction. The minimum and incremental values of vorticity contours are (±3 and 3 s^{-1}, respectively for all vorticity contours.

Reynolds stresses shown at the third column of Fig. 2 are normalized with the square root of the free-stream velocity. In Reynolds shear stress contours, patterns of negative Reynolds stress are indicated with dashed lines, on the other hand, patterns of positive Reynolds stress are indicated with solid lines. Minimum and incremental values of Reynolds shear stress are ±0.01 and 0.005, respectively for all $\langle u'v' \rangle / U^2$ concentrations. Pronounced concentrations of $\langle u'v' \rangle / U^2$ occur downstream of the base of the circular cylinder as a result of Karman Vortex shedding. There is a small scale Reynolds shear stress concentration downstream of the circular cylinder due to small magnitudes of fluctuations in the near wake of the circular cylinder. The peak concentration is approximately 0.146 and it occurs at 1.2 cylinder diameter downstream of the base of the circular cylinder. In terms of vortex shedding frequency, as a result of the FFT analysis of instantaneous velocity vector field obtained by the PIV, vortex shedding occurs at a natural frequency of 0.53 Hz.

To elucidate the effect of splitter plate length and height, experiments were carried out for four different lengths L/D = 0.5, 1.0, 1.5, 2.0 and for three different height ratios h_p/h_w = 0.25, 0.50, 0.75. Moreover, the height ratio of h_p/h_w = 1.0 was also studied for L/D = 1.0 and 2.0 cases. Flow structures for plate lengths of L/D = 0.5, 1.0, 1.5 and 2.0 are presented in Figs. 3–6, respectively. First columns of all figures demonstrate the time-averaged velocity vector fields. The second columns (b) and third columns (c) indicate time-averaged spanwise vorticity contours and Reynolds shear stress concentrations, respectively. For all cases of L/D, the effect of the splitter plate on the suppression of vortex shedding increases as the ratio of h_p/h_w increases. As a general trend for all figures, the wake region elongates along the streamwise direction with increasing the ratio of h_p/h_w and this elongation of the wake region is a sign of the significant attenuation of the large-scale vortex formation downstream of the circular cylinder. As the circulation region becomes larger, an increase occurs in the suction base pressure which is a sign of a decrease in the drag coefficient [23]. The distance of saddle point from the base of the circular cylinder is also an evidence of the degree of near wake extension. Substantial variation of the saddle point location, *Sa*, shows the height effect of the splitter plate on the flow characteristics. While the length of wake region is approximately 1*D* from the base of the cylinder for the bare cylinder case, it takes values of 1.16*D*, 1.35*D* and 1.7*D* for h_p/h_w = 0.25, 0.5 and 0.75 cases for the length of L/D = 0.5 (Fig. 3), respectively. Since, the prevention of the interaction of shear layers by the splitter plate is more pronounced with increasing h_p/h_w, the saddle point, *Sa* moves further away from the base of the cylinder with increasing h_p/h_w ratio. When the lowest height ratio h_p/h_w = 0.25 for L/D = 0.5 is compared to the same height ratio of L/D = 1.0, it is seen that the saddle point Sa moves away from a location of 1.16 *D* to 1.3 *D*. Furthermore, it occurs at a location of 2.18 *D* for the case of h_p/h_w = 1.0 for L/D = 1. When velocity vector fields of

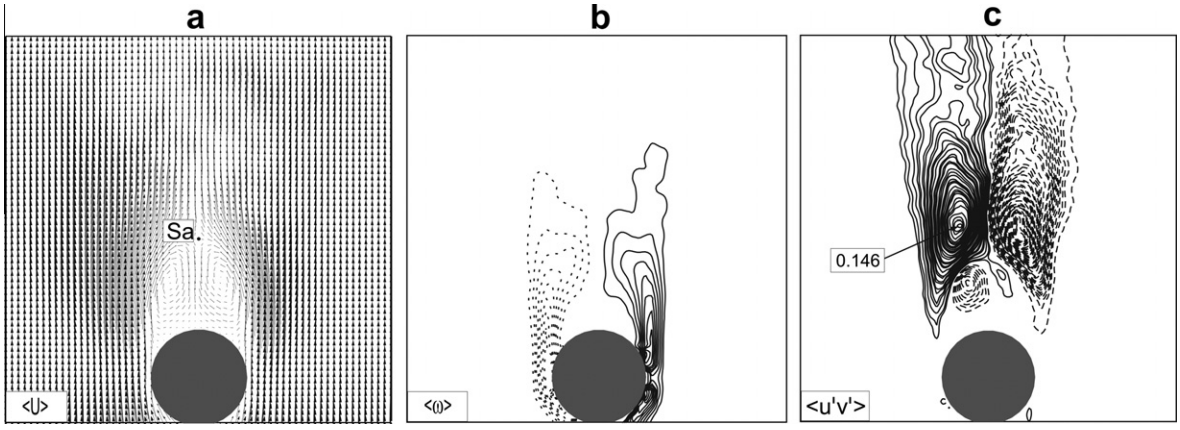

Fig. 2. Time-averaged flow structures behind a bare cylinder. (a) Velocity vector field downstream of the cylinder. (b) Patterns of spanwise vorticity contours. (c) Contours of normalized Reynolds stress.

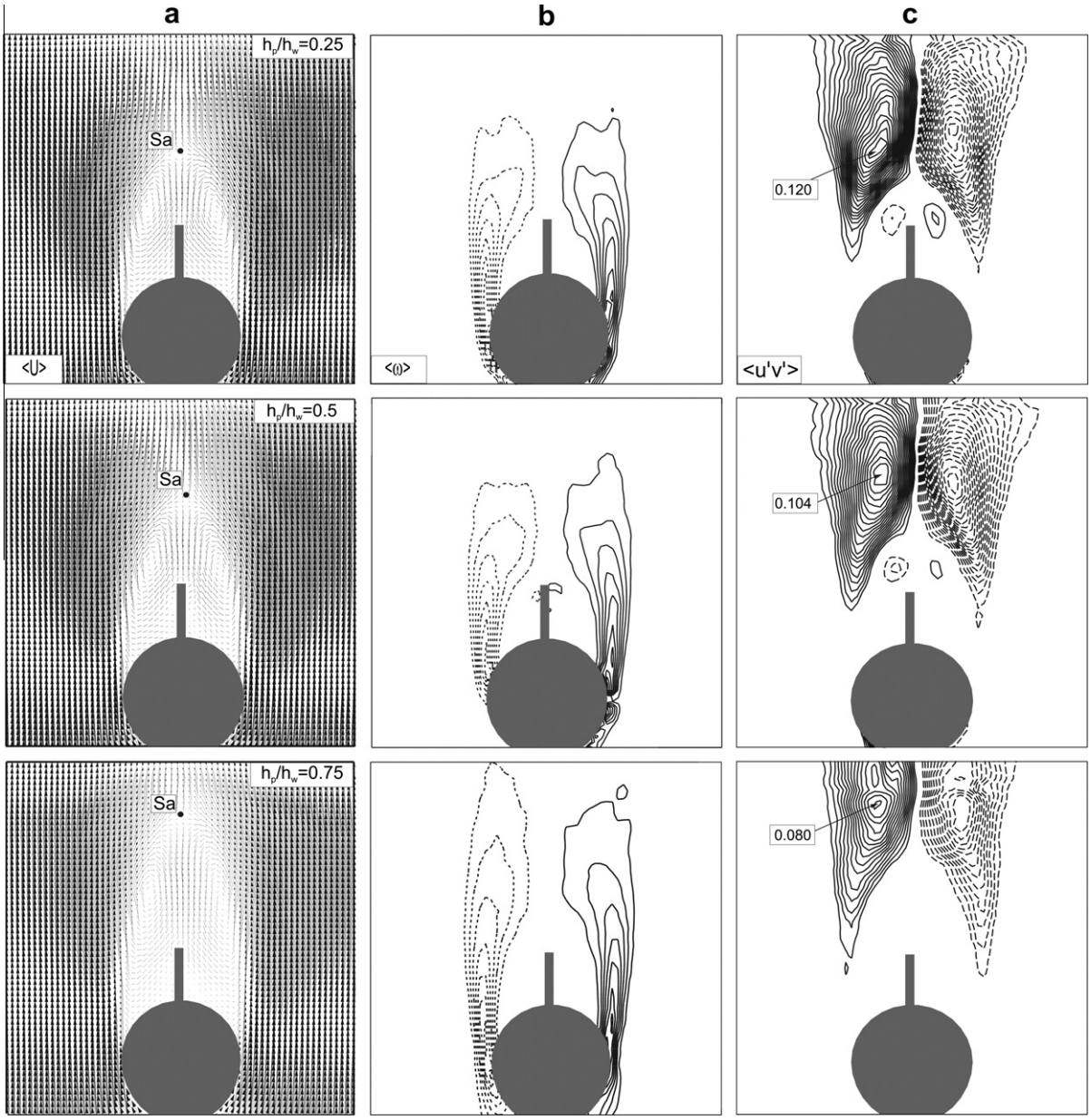

Fig. 3. (a) The time-averaged velocity vector field for $L/D = 0.5$. (b) Corresponding patterns of spanwise vorticity contours. Minimum and incremental values of vorticity are $\omega_{min} = \pm 3$ and $\Delta\omega = 3\ s^{-1}$. (c) Contours of normalized Reynolds stress. Minimum and incremental values of Reynolds stress are $[\langle u'v'\rangle/U^2]_{min} = \pm 0.01$ and $\Delta[\langle u'v'\rangle/U^2] = 0.005$.

lengths of $L/D = 2.0$ are observed, it is seen obviously that the locations of saddle points for the cases of $h_p/h_w = 0.75$ and 1.0 are located outside of the vector field of view.

In terms of spanwise vorticity contours shown in the second columns of the Figs. 3–6, with increasing h_p/h_w, positive and negative vorticity layers elongate in the streamwise direction regardless of plate length. Moreover, the decrease of the peak value of vorticity with increasing h_p/h_w indicates that the strength of the vortex shedding becomes weaker. Due to the effect of the splitter plate, the interaction between the core flow and wake region reduces. Therefore, the magnitude of the vorticity decreases compared to the bare cylinder case. For the height ratio of $h_p/h_w = 0.25$ for $L/D = 0.5$, the positive and negative vorticity layers get closer to each other after the trailing edge of the splitter plate as all cases of $h_p/h_w = 0.25$ for all plate lengths. The magnitude of vorticity layers for all height ratios of $L/D = 0.5$ changes slightly in spite of the fact that the vorticity contours get longer in streamwise direction with the increments of the ratio of h_p/h_w. For the case of $L/D = 1.0$, the elongation of the negative and positive vorticity layers is greater than that of $L/D = 0.5$ as illustrated in

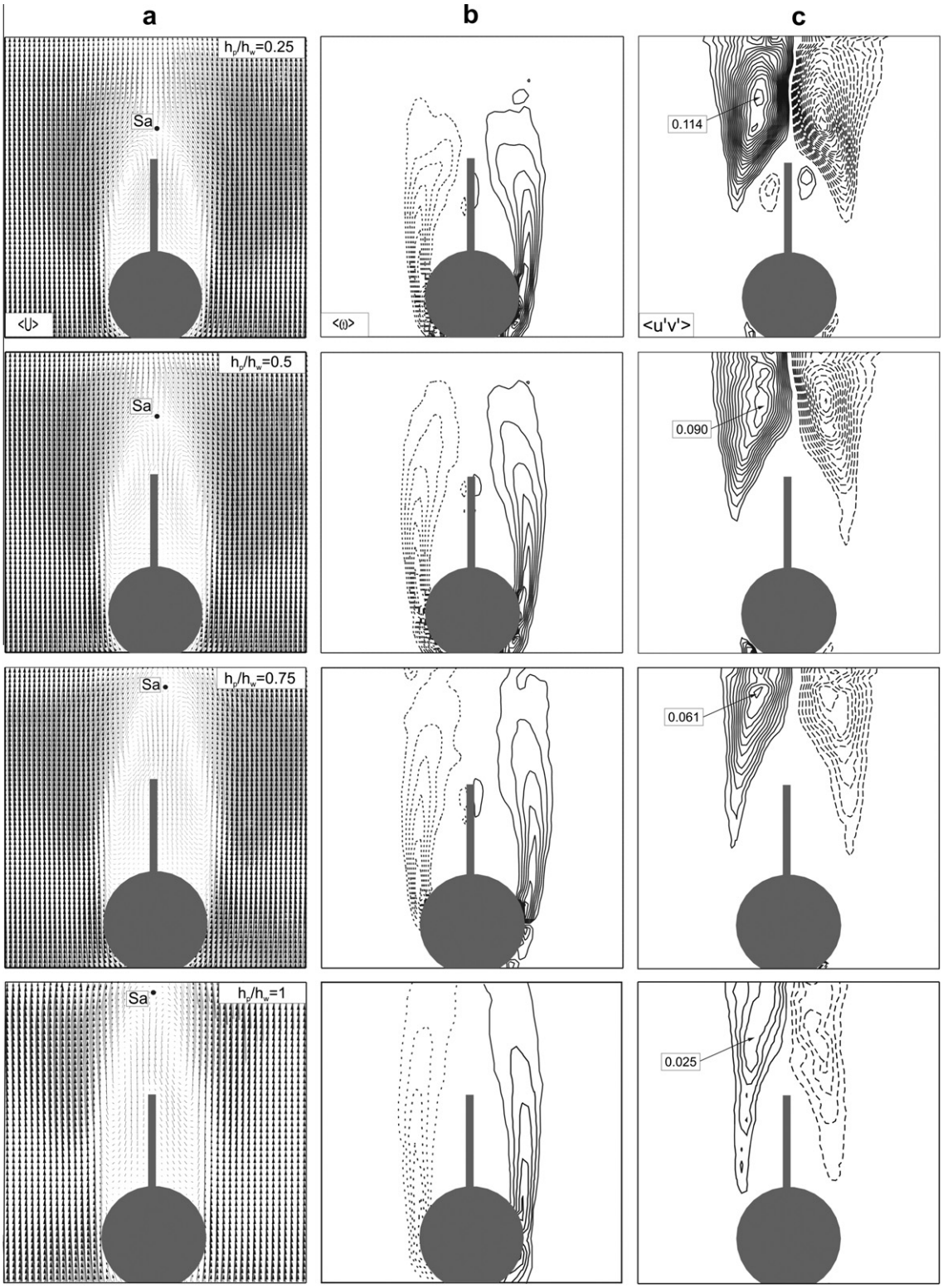

Fig. 4. (a) The time-averaged velocity vector field for $L/D = 1$. (b) Corresponding patterns of spanwise vorticity contours. Minimum and incremental values of vorticity are $\omega_{min} = \pm 3$ and $\Delta\omega = 3\ s^{-1}$. (c) Contours of normalized Reynolds stress. Minimum and incremental values of Reynolds stress are $[\langle u'v'\rangle/U^2]_{min} = \pm 0.01$ and $\Delta[\langle u'v'\rangle/U^2] = 0.005$.

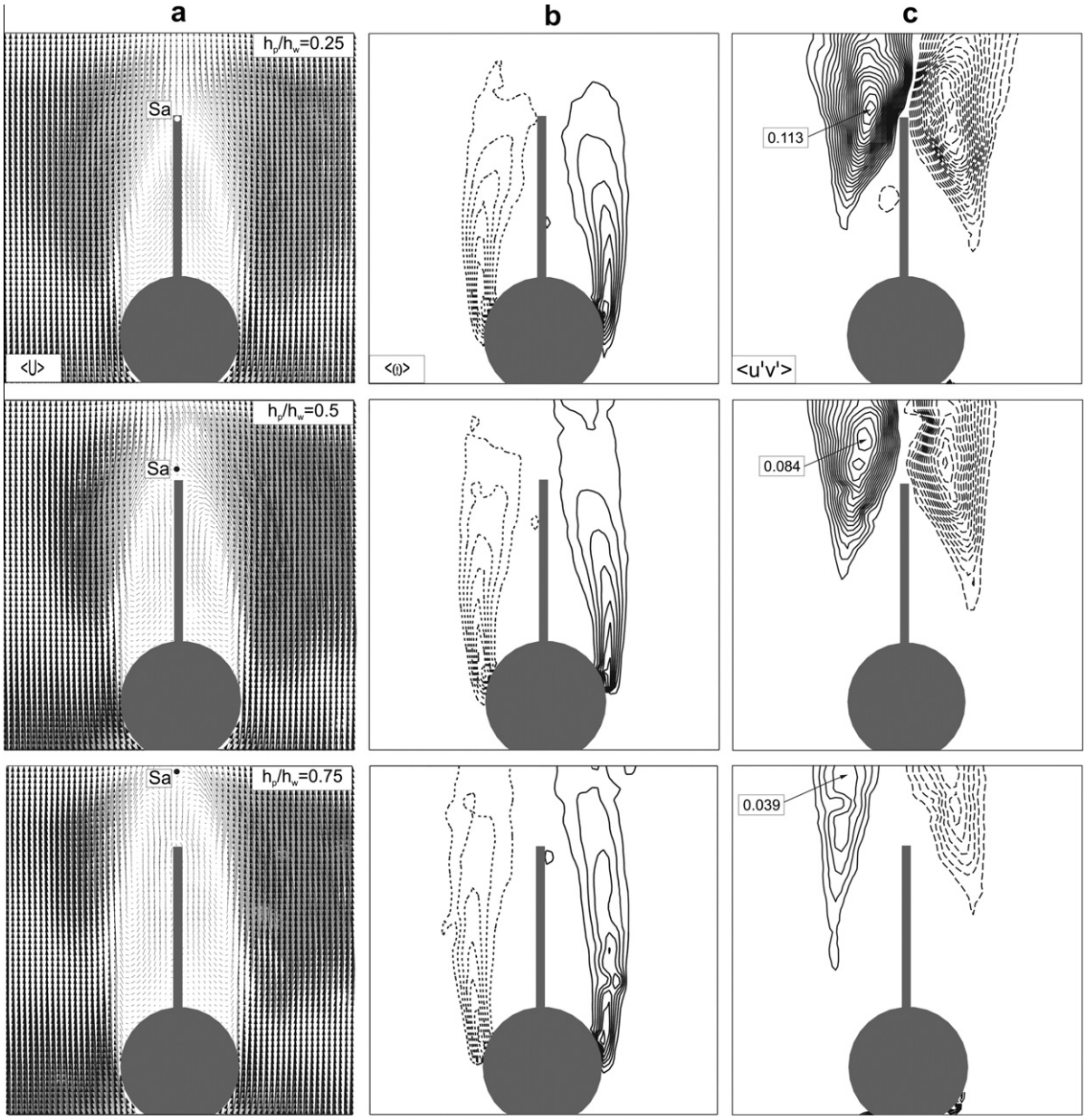

Fig. 5. (a) The time-averaged velocity vector field for $L/D = 1.5$. (b) Corresponding patterns of spanwise vorticity contours. Minimum and incremental values of vorticity are $\omega_{min} = \pm 3$ and $\Delta\omega = 3\ s^{-1}$. (c) Contours of normalized Reynolds stress. Minimum and incremental values of Reynolds stress are $[\langle u'v'\rangle/U^2]_{min} = \pm 0.01$ and $\Delta[\langle u'v'\rangle/U^2] = 0.005$.

Fig. 5. Due to the prevention of the interaction of the opposing shear layers, vorticity contours lengthen along the streamwise direction for the cases of $L/D = 1.5$ and 2. Especially for the cases of $h_p/h_w = 0.75$, 1.0 for $L/D = 2$ and the case of $h_p/h_w = 0.75$ for $L/D = 1.5$, the greater extension of vorticity layers than that of all cases is obtained and the negative and positive vorticity layers remain horizontal. This also shows the prevention of the momentum transfer from the free-stream flow into the wake region.

In Figs. 3–6, the third column shows the normalized Reynolds shear stress concentrations. Here, solid lines represent positive Reynolds shear stress contours while dashed lines show negative contours. All Reynolds shear stress concentrations are nearly symmetrical with two peaks located both sides of the splitter plate. When the ratio of h_p/h_w increases from 0.25 to 0.75, the magnitude of maximum $\langle u'v'\rangle/U^2$ decreases from 0.12 to 0.08 for the length of $L/D = 0.5$. Furthermore, small-scale Reynolds shear stresses downstream of the splitter plate disappear for the case of $h_p/h_w = 0.75$ and the location of peak concentration moves further downstream as the height ratio h_p/h_w increases. It is seen for the splitter plate having the

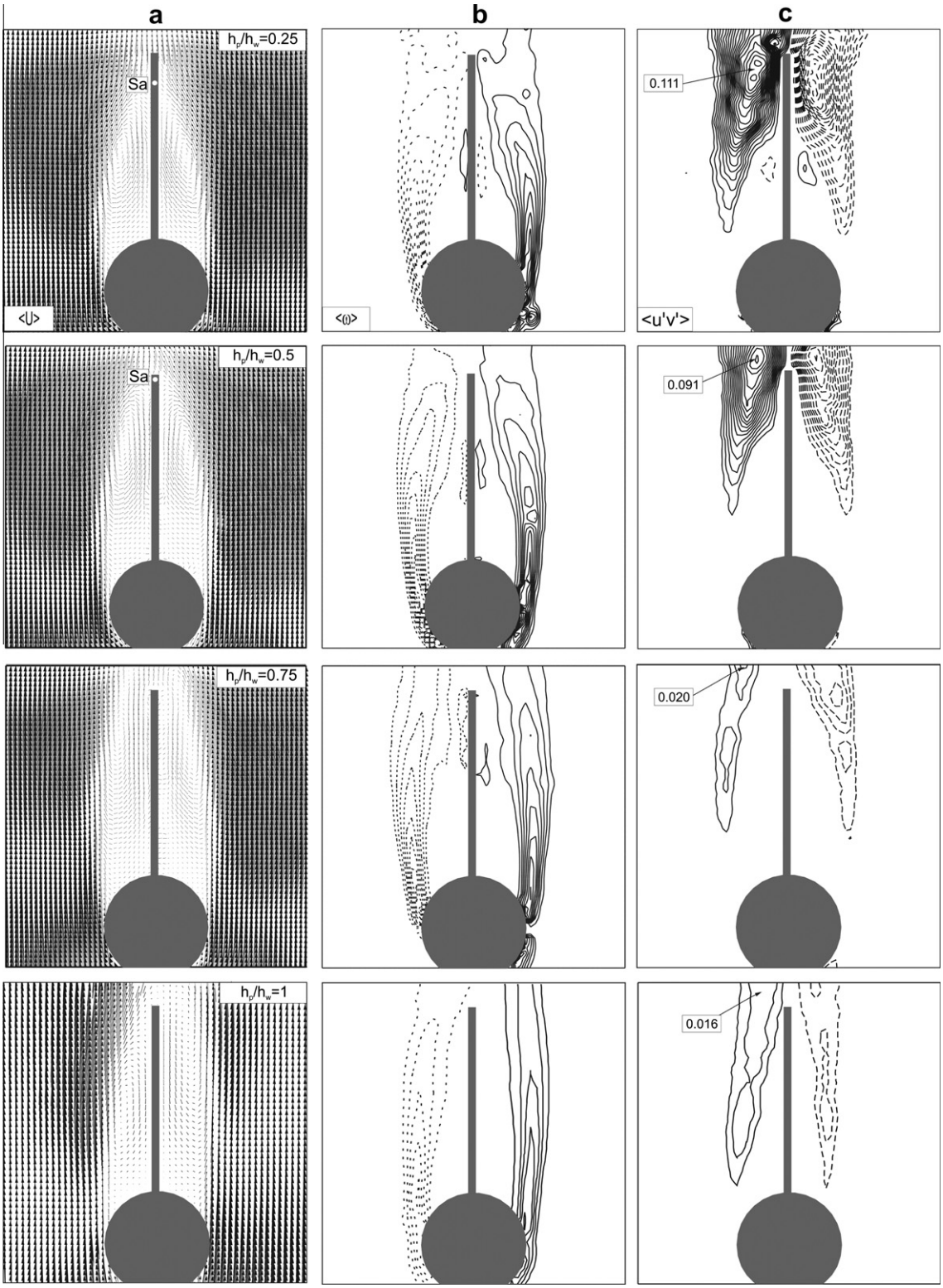

Fig. 6. (a) The time-averaged velocity vector field for $L/D = 2.0$. (b) Corresponding patterns of spanwise vorticity contours. Minimum and incremental values of vorticity are $\omega_{min} = \pm 3$ and $\Delta\omega = 3\ s^{-1}$. (c) Contours of normalized Reynolds stress. Minimum and incremental values of Reynolds stress are $[\langle u'v'\rangle/U^2]_{min} = \pm 0.01$ and $\Delta[\langle u'v'\rangle/U^2] = 0.005$.

length of $L/D = 1.0$, the magnitude of peak Reynolds shear stress diminishes considerably with increasing h_p/h_w. Small-scale Reynolds shear stresses are obtained for the length of $h_p/h_w = 0.25$ at a location of approximately 1 D which is very close to the trailing edge of the splitter plate, whereas these clusters disappear for other height ratios of $L/D = 1.0$. The magnitude of peak $\langle u'v' \rangle/U^2$ for the case of $h_p/h_w = 0.25$ for the length $L/D = 1.0$ is approximately 0.114 which is less than that of the case of $h_p/h_w = 0.25$ for $L/D = 0.5$. For the height ratio of $h_p/h_w = 1.0$ for $L/D = 1.0$, a value of 0.025 which is nearly six times smaller than that of the bare cylinder case is obtained. Moreover, the location of peak Reynolds shear stress moves away from the base of the cylinder and the location of the peak $\langle u'v' \rangle/U^2$ is observed further away from the centerline with increasing the plate height. The location of peak $\langle u'v' \rangle/U^2$ for the cases of $h_p/h_w = 0.75$ and 1.0 for $L/D = 2$ is more than two cylinder diameters away from the base of the circular cylinder. Furthermore, as a result of the suppression of unsteady vortices formed in the near wake of the circular cylinder, the magnitude of the Reynolds shear stress decreases with increasing height ratio. The peak concentrations of $\langle u'v' \rangle/U^2$ for $h_p/h_w = 0.25$, 0.5, 0.75 and 1.0 for $L/D = 2$ are attenuated to the values of 0.142, 0.091, 0.020 and 0.016, respectively. This considerable decrease in the Reynolds shear stress is obtained due to the reduction in the drag force of the circular cylinder [31].

3.2. Effect of normalized transverse and streamwise Reynolds normal stresses

The variation of peak values of the normalized transverse ($\langle v'v' \rangle/U^2$) and streamwise ($\langle u'u' \rangle/U^2$) Reynolds normal stresses based on the plate length (L/D) for all height ratios (h_p/h_w) are given in Fig. 7 to demonstrate their effect on the decay of turbulent kinetic energy.

Since peak value of the normalized transverse Reynolds normal stress ($\langle v'v' \rangle/U^2$) for the case of $h_p/h_w = 0.75$ for $L/D = 2$ occurs out of the flow domain obtained by PIV, the peak value was estimated and indicated by dashed line in the figure. It is apparent that increasing height ratio results in a decrease in the peak value of both $\langle u'u' \rangle/U^2$ and $\langle v'v' \rangle/U^2$. The peak values of $\langle u'u' \rangle/U^2$ and $\langle v'v' \rangle/U^2$ for the bare cylinder case are 0.237 and 0.38, respectively. The peak value of the normalized transverse Reynolds normal stress for $L/D = 0.5$ decreases to values of 0.29, 0.26 and 0.15 for the height ratios of $h_p/h_w = 0.25$, 0.5 and 0.75, respectively. The peak values of the normalized streamwise Reynolds normal stress for the same plate length and height ratios drop to 0.173, 0.171 and 0.15. When the plate length is increased to $L/D = 2$ for the height ratio of $h_p/h_w = 0.75$, the peak values of $\langle u'u' \rangle/U^2$ and $\langle v'v' \rangle/U^2$ decrease to the values of 0.078 and 0.036, respectively. Fig. 7 shows that the peak value of transverse Reynolds normal stress changes dramatically until $L/D = 1.5$. However, the peak value changes inconsiderably from $L/D = 1.5$ to $L/D = 2.0$. Fig. 7 also indicates that the variation of the peak value of $\langle u'u' \rangle/U^2$ depending on the change in L/D is small compared to the $\langle v'v' \rangle/U^2$. These numerical values represent that the transverse Reynolds normal stress has significant effect on the alleviation of turbulent kinetic energy compared to the streamwise Reynolds normal stress.

In Fig. 8, the normalized transverse Reynolds normal stress contours for $h_p/h_w = 0.75$ at different plate lengths (L/D) are addressed to display the effect of splitter plate length on the flow characteristics. The minimum and incremental values of the contours for normalized transverse Reynolds normal stress are 0.01 and 0.005, respectively. The transverse Reynolds normal stress increases along the downstream direction starting from the base of the circular cylinder until it reaches its peak value at a location very close to the saddle point along the centerline in the wake region for $L/D = 0.5$ and 1.0. While single peak occurs for $L/D = 0.5$ and 1.0 cases, a double-peak is obtained for $L/D = 1.5$ and 2.0 cases, as a result of the prevention of the interaction of shear layers. Both shear layers do not communicate each other and behave independently with the presence of the plate. Therefore, the peak value of $\langle v'v' \rangle/U^2$ does not occur along the centerline anymore. The peak value of transverse Reynolds normal stress shows a decrease with increasing plate length. While the peak value of transverse Reynolds normal stress for bare cylinder case is about 0.38, it decreases to 0.15, 0.11 and 0.041for $L/D = 0.5$, 1 and 1.5, respectively. In terms of $L/D = 2$ case,

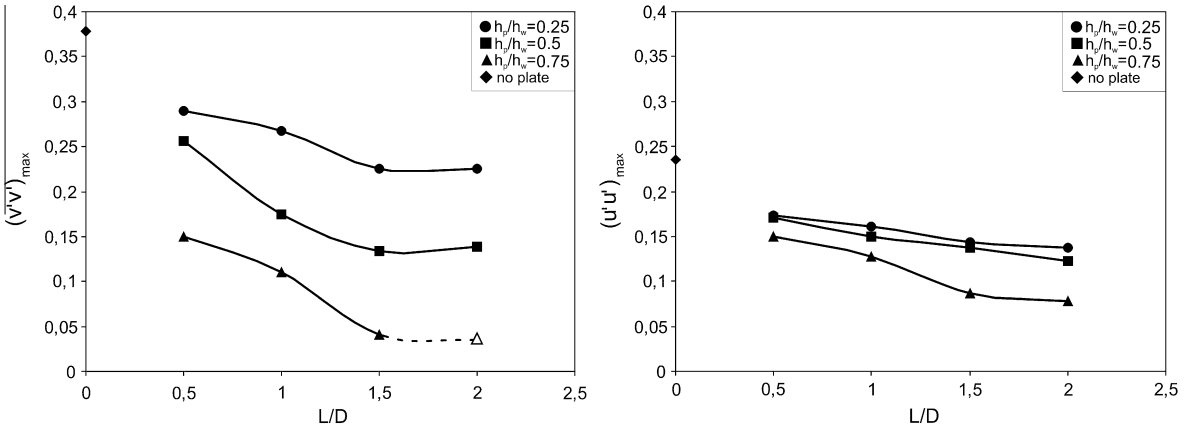

Fig. 7. The variation of peak values of the normalized transverse and streamwise Reynolds normal stress based on the plate length (L/D) for all plate heights (h_p/h_w). Estimated peak value for $h_p/h_w = 0.75$ for $L/D = 2$ is shown with dashed line.

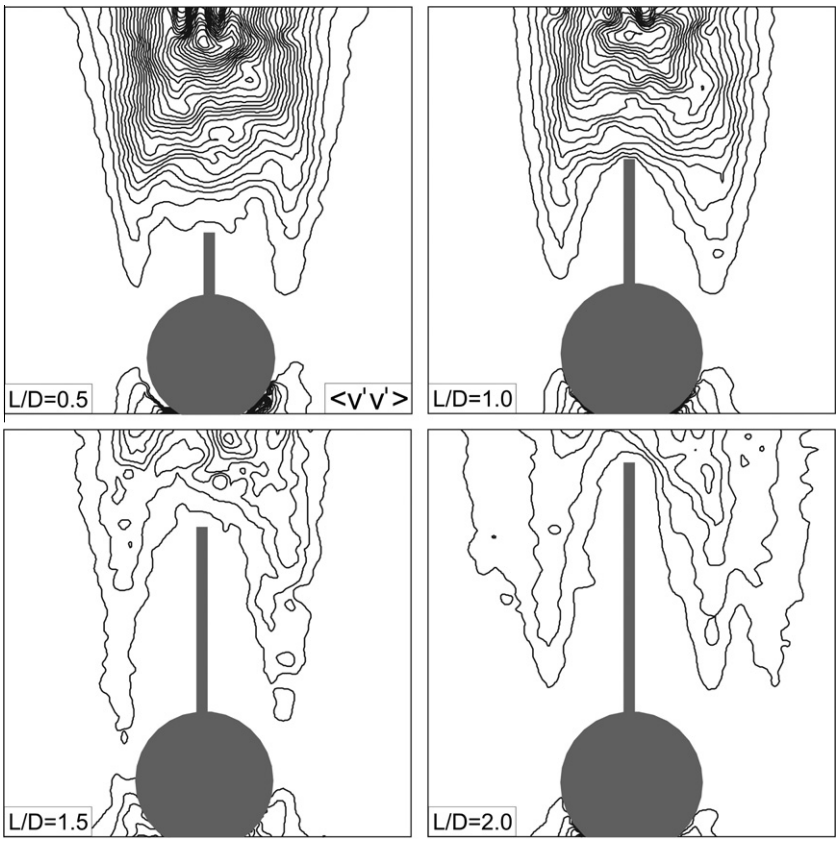

Fig. 8. Normalized transverse Reynolds normal stress $\langle v'v' \rangle / U^2$ of the plate height of $h_p/h_w = 0.75$ for different plate lengths (L/D).

the peak transverse Reynolds normal stress moves out of field of view obtained from PIV. Therefore, the peak value of $\langle v'v' \rangle / U^2$ for $L/D = 2$ was estimated from the contour plots as 0.036. The location of peak value of $\langle v'v' \rangle / U^2$ changes slightly with the change in the splitter plate length.

Fig. 9 presents the variation of peak turbulent kinetic energy (TKE) as a function of L/D for different plate heights. The peak value of TKE decreases progressively compared to the bare cylinder case. While the peak value of TKE for the bare cylinder case is approximately 0.38, the peak value of TKE for the smallest plate length, that is $L/D = 0.5$, decreases to approximately 0.26 for all splitter plate height ratios. The peak value of TKE starts to decrease with increasing L/D ratio for all height ratios. However, this decrease is more pronounced for the largest height ratio, $h_p/h_w = 0.75$. The decrease in the peak value of TKE means that the presence of splitter plate downstream of the circular cylinder strongly suppresses the large scale vortices, which carry fresh fluid from free-stream region into the wake region. For the height ratios of $h_p/h_w = 0.5$ and 0.75, peak values of TKE for the length of $L/D = 2$ decrease to 0.14 and 0.036, respectively. The transverse Reynolds normal stress is more effective on the attenuation of turbulent kinetic energy than the streamwise Reynolds normal stress. The value of peak transverse Reynolds normal stress is reduced to 90% of that of the bare cylinder at most. However, the

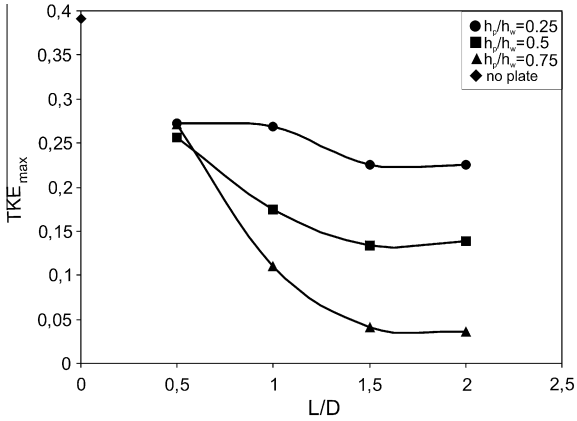

Fig. 9. The relationship between peak magnitude of turbulent kinetic energy TKE_{max} and L/D for different plate heights h_p/h_w.

variation of TKE for the height ratio of $h_p/h_w = 0.25$ shows a small difference compared to other two height ratios although the peak values of TKE for this height ratio are obviously less than that of bare cylinder case.

3.3. Effect of splitter plate on the vortex shedding frequency

Spectra of streamwise velocity fluctuations displayed in Fig. 10 are evaluated at a certain location for different plate

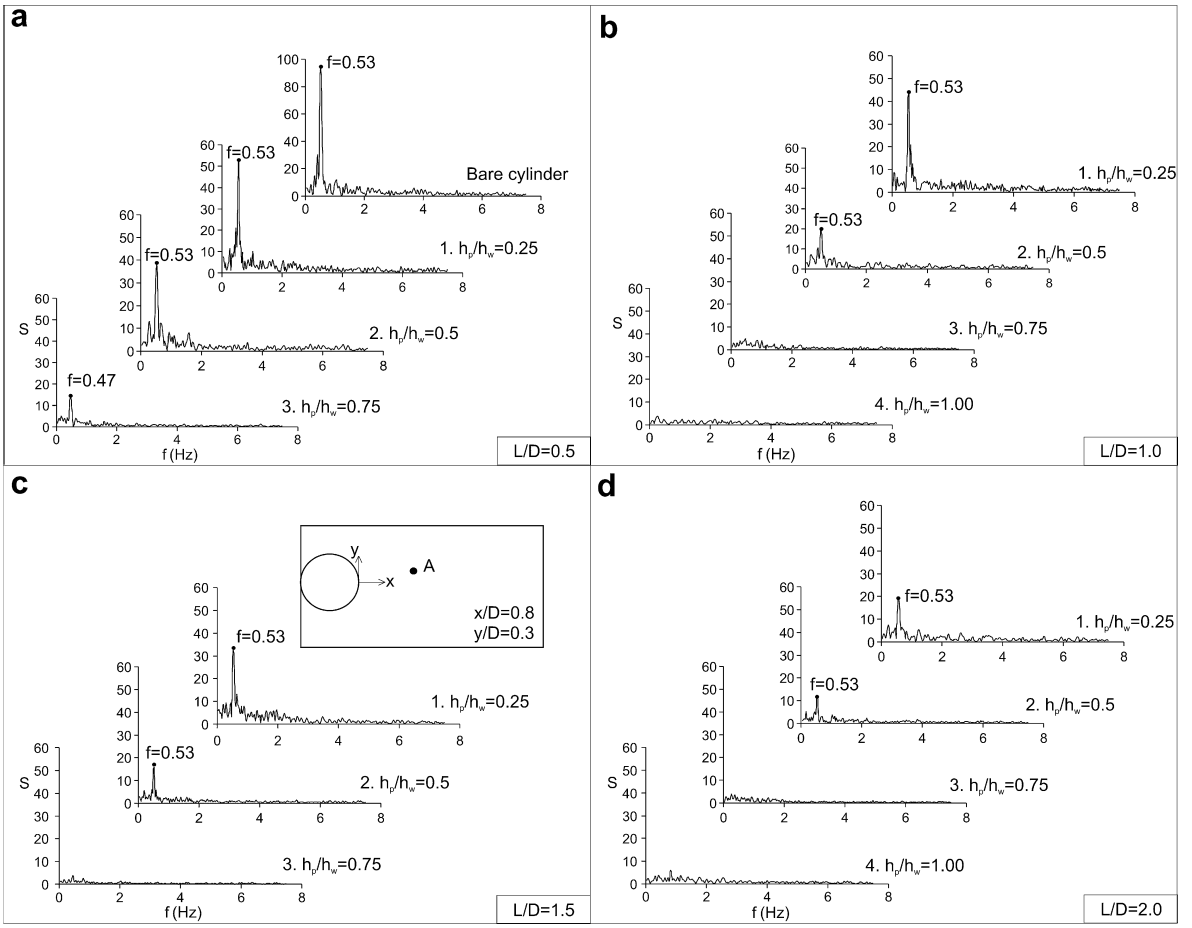

Fig. 10. Comparison of vortex shedding frequencies with varying splitter plate heights and lengths at a certain location. (a) Vortex shedding frequencies of the plate length of $L/D = 0.5$. (b) Vortex shedding frequencies of the plate length of $L/D = 1.0$. (c) Vortex shedding frequencies of the plate length of $L/D = 1.5$. (d) Vortex shedding frequencies of the plate length of $L/D = 2.0$.

lengths and height ratios. The location of A at which spectra is taken, is presented in the left bottom section of Fig. 10 as $x/D = 0.8$ and $y/D = 0.3$. Natural frequency of vortex shedding is 0.53 Hz for bare cylinder case as seen in Fig. 10a. For the smallest splitter plate length ($L/D = 0.5$), the vortex shedding occurs at the natural frequency of vortex shedding of bare cylinder for $h_p/h_w = 0.25$ and 0.5. However, the frequency of vortex shedding decreases to a value of 0.47 Hz for $h_p/h_w = 0.75$. Furthermore, the magnitude of the spectra decreases with increasing height ratio. It should be noted that as h_p/h_w increases, the dominant peaks in the power spectra become less pronounced, confirming to the attenuated forces and weakened vortex shedding [32]. For other splitter plate lengths as seen Fig. 10b–d, no vortex shedding frequency occurs for $h_p/h_w = 0.75$ and 1.0 cases. It can be concluded that unsteady flow structure is considerably prevented with the presence of splitter plates having height ratio of $h_p/h_w = 0.75$ for $L/D \geqslant 1.0$.

Fig. 11 indicates the variation of the saddle point location as a function of splitter plate length at various height ratios. The wake region downstream of the circular cylinder elongates considerably along the streamwise direction

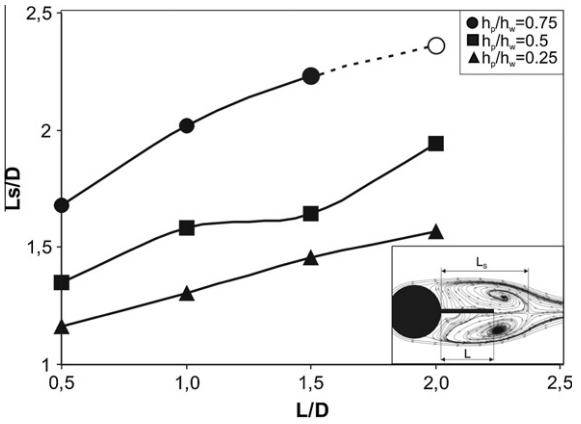

Fig. 11. Variation of saddle point location as a function of splitter plate length. Estimated location of saddle point for $h_p/h_w = 0.75$ for $L/D = 2$ is indicated by dashed line.

with increasing of h_p/h_w. Therefore, the location of saddle point, *Sa*, moves downstream as h_p/h_w increases. Since saddle point location for the case of $h_p/h_w = 0.75$ for $L/D = 2$ oc-

curs out of the flow domain obtained by PIV, estimated location of saddle point was indicated by dashed line. When the effect of the splitter plate length is considered, it can be seen that increasing splitter plate length results in an increase in the vortex formation length.

4. Conclusions

The experimental study presented herein reveals the effect of the splitter plates having different heights and lengths located in the wake region of the circular cylinder in shallow water flow. Time-averaged patterns of velocity vectors, spanwise vorticity and Reynolds shear stress contours, obtained from PIV measurements, were used to explain the flow structure downstream of the circular cylinder. The results obtained in this study demonstrate that the mean flow and turbulent quantities change considerably with height and length ratios of the splitter plates in shallow flow as a result of the prevention of interaction of shear layers located on both sides of the cylinder. Karman vortex shedding is attenuated pronouncedly for the cases of $L/D \geqslant 1$ and $h_p/h_w \geqslant 0.75$. The most effective case on the control of vortex shedding is the case of the plate length of $L/D = 2$ compared to other cases. In terms of height ratio, the $h_p/h_w = 1$ case is the most effective one relative to the other height ratios. Wake region downstream of the cylinder elongates substantially along the streamwise direction with increasing splitter plate length since the splitter plate prevents the interaction of the separated shear layer on both sides of the cylinder. The Reynolds stress concentrations decrease substantially with the presence of splitter plate compared to the bare cylinder case. Furthermore, any dominant frequency of vortex shedding for all plate lengths is not observed when the plate height is greater than the height ratio of $h_p/h_w = 0.5$. For all plate lengths, the case of $h_p/h_w = 0.5$ has a significant effect on the suppression of vortex shedding although its influence is less than that obtained for the cases of $h_p/h_w = 0.75$ and 1. In addition, the transverse Reynolds normal stress has more influence on the attenuation of turbulent kinetic energy than the streamwise Reynolds normal stress for all plate heights and lengths.

Acknowledgement

The authors would like to acknowledge the financial support of the Scientific and Technological Research Council of Turkey for funding under Contract No. 105M267.

References

[1] N. Fujisawa, Feedback control of vortex shedding from a circular cylinder by rotational oscillations, J. Fluid Struct. 15 (2001) 23–37.
[2] T. Weier, G. Gerbeth, G. Mutschke, E. Platacis, O. Lielausis, Experiments on cylinder wake stabilization in an electrolyte solution by means of electromagnetic forced localized on the cylinder surface, Exp. Therm Fluid Sci. 16 (1998) 84–91.
[3] S. Kang, H. Choi, Laminar flow past a rotating circular cylinder, Phys. Fluids 11 (1999) 12–21.
[4] D. Shiels, A. Leonard, Investigation of a drag reduction on a circular cylinder in rotary oscillation, J. Fluid Mech. 431 (1993) 297–322.
[5] E. Guilmineau, P. Queutey, A numerical simulation of vortex shedding from an oscillating circular cylinder, J. Fluid Struct. 16 (2002) 773–794.
[6] Z. Li, I.M. Navon, M.Y. Hussaini, F.-X. Le Dimet, Optimal control of cylinder wakes via suction and blowing, Comput. Fluids 32 (2003) 149–171.
[7] B.S.V. Patniak, G.W. Wei, Controlling wake turbulence, Phys. Rev. Lett. 88 (2002) 054502.
[8] Y. Delaunay, L. Kaiktsis, Control of circular cylinder wakes using base mass transpiration, Phys. Fluids 13 (2001) 3285–3302.
[9] S. Ozono, Flow control of vortex shedding by a short splitter plate asymmetrically arranged downstream of a cylinder, Phys. Fluids 11 (1999) 2928–2934.
[10] J.M. Cimbala, S. Garg, Flow in the wake of a freely rotatable cylinder with splitter plate, AIAA J. 29 (1991) 1001–1003.
[11] G.S. Cardell, Flow past a circular cylinder with a permeable wake splitter plate, Ph.D. Thesis, California Institute of Technology, 1993.
[12] K. Kwon, H. Choi, Control of laminar vortex shedding behind a circular cylinder using splitter plates, Phys. Fluids 8 (1996) 479–486.
[13] H. Akilli, B. Sahin, N.F. Tumen, Suppression of vortex shedding of circular cylinder in shallow water by a splitter plate, Flow Meas. Instrum. 16 (2005) 211–219.
[14] H. Akilli, C. Karakus, A. Akar, B. Sahin, N.F. Tumen, Control of vortex shedding of circular cylinder in shallow water flow using an attached splitter plate, J. Fluid Eng – Trans. ASME 130 (2008) 1–11.
[15] S.J. Lee, S.I. Lee, C.W. Park, Reducing the drag on a circular cylinder by upstream installation of a small control rod, Fluid Dyn. Res. 34 (2004) 233–250.
[16] P.R. Bandyopadhyay, Review-mean flow in turbulent boundary layers disturbed to alter skin friction, J. Fluids Eng. 108 (1986) 127–140.
[17] H.-C. Lim, S.-J. Lee, Flow control of a circular cylinder with o-rings, Fluid Dyn. Res. 35 (2004) 107–122.
[18] H. Fu, D. Rockwell, Shallow flow past a cylinder: control of the near wake, J. Fluid Mech. 539 (2005) 1–24.
[19] R.G. Ingram, V.H. Chu, Flow around island in Rupert Bay: an investigation of the bottom friction effect, J. Geophys. Res. 92 (1987) 14521–14533.
[20] D. Chen, H. Jirka, Experimental study of plane turbulent wakes in a shallow water layer, Fluid Dyn. Res. 16 (1995) 11–41.
[21] H. Akilli, A. Akar, C. Karakus, Flow characteristics of circular cylinders arranged side-by-side in shallow water, Flow Meas. Instrum. 15 (2004) 187–197.
[22] H. Akilli, D. Rockwell, Vortex formation from a cylinder in shallow water, Phys. Fluids 14 (2002) 2957–2967.
[23] J.E. Jaramillo, C.D. Perez-Segarra, J. Castro, O. Lehmkuhl, Detailed analysis of turbulent flows in air curtains, Prog. Comput. Fluid Dyn. 11 (2011) 350–362.
[24] H. Choi, W.-P. Jean, J. Kim, Control of flow over a bluff body, Annu. Rev. Fluid Mech. 40 (2008) 113–139.
[25] C.H.K. Williamson, Vortex – induced vibration, Annu. Rev. Fluid Mech. 36 (2004) 413–455.
[26] R.A.D. Akkermans, A.R. Cieslik, L.P.J. Kamp, R.R. Trieling, H.J.H. Clercx, G.J.F. van Heijst, The three-dimensional structure of an electromagnetically generated dipolar vortex in a shallow fluid layer, Phys. Fluids 20 (2008) 116601–1166014.
[27] R.A.D. Akkermans, L.P.J. Kamp, H.J.H. Clercx, G.J.F. van Heijst, Intrinsic three-dimensionality in electromagnetically driven shallow flows, EPL 83 (2008) 24001.
[28] R.A.D. Akkermans, A.P.C. Holten, L.P.J. Kamp, H.J.H. Clercx, G.J.F. van Heijst, Arrays of vortices in shallow fluids: three-dimensional structure and dispersion, Eur. J. Mech. B – Fluid 34 (2012) 131–145.
[29] D. Sous, N. Bonneton, J. Sommeria, Transition from deep to shallow water layer: formation of vortex dipoles, Eur. J. Mech. B-Fluid 24 (2005) 19–32.
[30] J.-C. Lin, M. Ozgoren, D. Rockwell, Space–time development of the onset of a shallow-water vortex, J. Fluid Mech. 485 (2003) 33–66.
[31] W. Kim, J.Y. Yoo, J. Sung, Dynamics of vortex lock-on in a perturbed cylinder wake, Phys. Fluids 18 (2006) 074103.
[32] J.C. Hu, Y. Zhou, Aerodynamic characteristics of asymmetric bluff bodies, J. Fluid ENG – T ASM 131 (2009) 011206.
[33] M. Raffel, C.E. Willert, J. Kompenhans, Particle Image Velocimetry a Practical Guide, Springer, Göttingen, 1998.